# Phase diagram of the spin S = 1/2 extended XY model

I. Titvinidze and G.I. Japaridze[a]

Andronikashvili Institute of Physics, Georgian Academy of Sciences Tamarashvili str. 6, 380077, Tbilisi, Georgia

**Abstract.** The quantum phase transition in the ground state of the extended spin $S = 1/2$ $XY$ model has been studied in detail. Using the exact solution of the model the low temperature thermodynamics, as well as the ground state phase diagram of the model in the presence of applied uniform and/or staggered magnetic field are discussed.

**PACS.** 71.27.+a Strongly correlated electron systems; heavy fermions – 75.10.Jm Quantized spin models

## 1 Introduction

There is a considerable interest in models of strongly correlated electron and spin systems showing a Quantum Phase Transition (QPT) (see Ref. [1]). In the case of One-Dimensional electron or spin systems QPT related to the dynamical generation of a charge or spin gap is often connected with the change in the topology of the Fermi surface, in particular with the doubling of the number of Fermi points [2–5].

The one-dimensional spin $S = 1/2$ $XY$ chain

$$\mathcal{H}_{XY} = -J \sum_n \left( S_n^x S_{n+1}^x + S_n^y S_{n+1}^y \right) \quad (1)$$

is the simplest exactly solvable strongly correlated spin model [6,7]. Its exact solution is expressed in terms of the *Fermi gas of spinless particles* (spinless Fermions (SF)). The free Fermi gas principle for construction of the system eigenstates and eigenvalues provides the straightforward and easy way to obtain the exact expressions for correlation functions and thermodynamic quantities (see Ref. [8] and references therein).

More than thirty years ago M. Suzuki proposed the whole class of generalized $XY$ models with multi-spin interaction, allowing the exact solution in terms of the *Fermi gas of spinless Fermions* [9]. In the fermionic representation, the multi-spin coupling shows itself only through the form of the single particle spectrum. In this paper we consider the simplest of the proposed generalized $XY$ models – the extended $XY$ model with three spin coupling. The
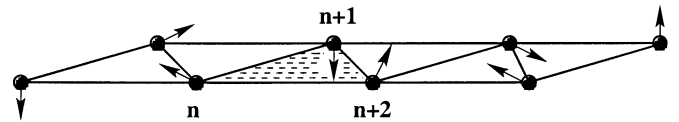
**Fig. 1.** Schematic representation of the structure of the extended $XY$ model.

Hamiltonian of the model is given by

$$\mathcal{H} = -J \sum_n \left( S_n^x S_{n+1}^x + S_n^y S_{n+1}^y \right)$$
$$- J^* \left( S_n^x S_{n+2}^x + S_n^y S_{n+2}^y \right) S_{n+1}^z \quad (2)$$

and describes the spin system determined on the zig-zag chain (see Fig. 1), with the transverse exchange between the spins on the nearest-neighbor sites $J$, and transverse exchange between the spins on the next-nearest-neighbor sites $J^*$, the latter depends on "$z$" orientation of the spin being between the next-nearest-neighbors.

Despite its rather formal and possibly even nonrealistic nature the model (2) attracted our attention owing to its several important advantages:

- it is an exactly solvable model;
- the exact solution is expressed in terms of Fermi gas of SF.

Moreover, as it is shown in this paper, the model (2) is characterized by the rich ground state phase diagram. In particular

- with the increase of three spin coupling, at $J_c^* = 2J$ the system experiences QPT from the *Spin Liquid I* phase into the *Spin Liquid II* phase;
- in the SF representation this QPT is associated with the doubling of Fermi points;

- at the transition point the magnetic and low-temperature thermodynamic properties of the system show a well pronounced anomalous behavior;
- in the case of applied uniform and/or staggered magnetic field the system is characterized by the rich ground state phase diagram which contains *ferromagnetic, antiferromagnetic and three different spin liquid phases.*

The paper is organized as follows. In the forthcoming section we discuss the spinless Fermion representation of the model. In the Section 3 the ground state properties are discussed. In the Section 4 the low-temperature thermodynamics of the system is considered. In the Section 5 the ground state phase diagram of the model is studied in the presence of magnetic field. Finally, the Section 6 contains the discussion and concluding remarks. The paper contains also two appendices. In Appendix A we present the table with exact expressions for the so called emptiness formation probability (EFP) $P(n)$ for $n = 1, ..., 20$ and for different values of the parameter $J^*$. In Appendix B we present the expression for the EFP, which fits our exact data for $\alpha \geq \alpha_c$.

## 2 Spinless fermion representation

The Hamiltonian (2) can be diagonalized by means of the Jordan-Wigner transformation [10]

$$S_n^+ = S_n^x + iS_n^y = \prod_{m=1}^{n-1} \left(1 - 2c_m^\dagger c_m\right) c_n^\dagger$$

$$S_n^- = S_n^x - iS_n^y = \prod_{m=1}^{n-1} c_n \left(1 - 2c_m^\dagger c_m\right)$$

$$S_n^z = c_n^\dagger c_n - \frac{1}{2} \tag{3}$$

where $c_n^\dagger, c_n$ are the spinless fermion (SF) creation and annihilation operators, respectively. In fact, the Hamiltonian (2) is transformed to a free spinless fermion model as

$$\mathcal{H} = -\frac{J}{2} \sum_n \left(c_n^\dagger c_{n+1} + c_{n+1}^\dagger c_n\right)$$

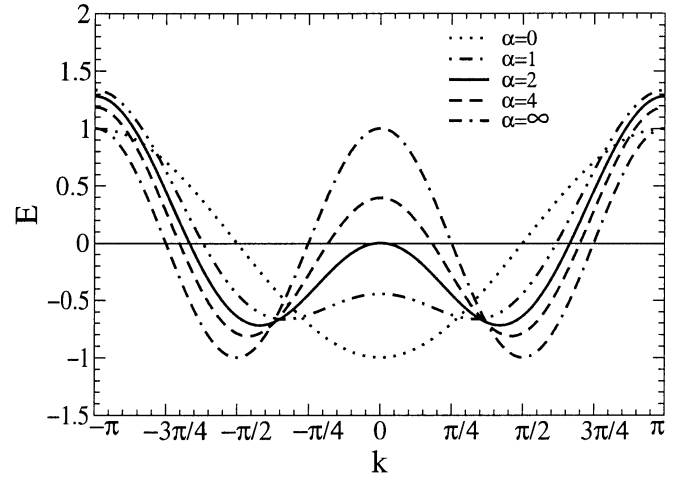$$+ \frac{J^*}{4} \sum_n \left(c_n^\dagger c_{n+2} + c_{n+2}^\dagger c_n\right). \tag{4}$$

We can diagonalize the Hamiltonian (4) by means of the Fourier transformation to obtain

$$\mathcal{H} = \sum_k E(k) c^\dagger(k) c(k) \tag{5}$$

where

$$E(k) = -J \left(\cos(k) - \frac{\alpha}{2} \cos 2k\right) \tag{6}$$

and $\alpha = J^*/J$.



**Fig. 2.** The spectra for different values of the parameter $\alpha$. For given $\alpha$ the corresponding curve is scaled so as to give the same bandwidth equal to 2.

In what follows we assume that $J > 0$ and $\alpha > 0$. However, since the unitary transformation

$$S_n^{x,y} \to (-1)^n S_n^{x,y}, \qquad S_n^z \to S_n^z \tag{7}$$

changes the sign of the nearest neighbor exchange constant $J \to -J$, one can easily reconstruct the features of the system for $J < 0$ using the transformation (7). Moreover, since the sign of the three spin coupling term is changed by the time reversal transformation

$$S_n^y \to S_n^y, \qquad S_n^{x,z} \to -S_n^{x,z}, \tag{8}$$

the properties of the system for $\alpha < 0$ can be easily obtained from the ground state phase diagram of the system at $\alpha > 0$ using the transformation (8).

In the thermodynamic limit ($N \to \infty$), the ground state of the system corresponds to the configuration where all the states with $E(k) \leq 0$ are filled and $E(k) > 0$ are empty. For $\alpha < 0.5$, the band minimum is at $k = 0$ (see Fig. 2). If $\alpha > 0.5$, the band minima $\pm k_{min}$ move away from $k = 0$ and satisfy the relation $\cos(k_{min}) = 1/2\alpha$, while a band maximum at $k = 0$ is $E(0) = J(\alpha/2 - 1)$. Therefore, for $\alpha < 2$ there are only two Fermi points at

$$\pm k_F^- = \arccos\left[\left(1 - \sqrt{1 + 2\alpha^2}\right)/2\alpha\right] \tag{9}$$

and the ground state corresponds to the configuration when all states with $|k| < k_F^-$ are filled. At $\alpha = \alpha_c = 2$ the band maximum at $k = 0$ reaches the Fermi level (see Fig. 2) and at $\alpha > \alpha_c$ $E(0) > 0$ and therefore, two additional Fermi points appear at

$$\pm k_F^+ = \arccos\left[\left(1 + \sqrt{1 + 2\alpha^2}\right)/2\alpha\right]. \tag{10}$$

In this case the ground state corresponds to the configuration when all states with $k_F^+ < |k| < k_F^-$ are filled.

As we show in this paper, the change of the topology of the Fermi surface of the equivalent SF model for
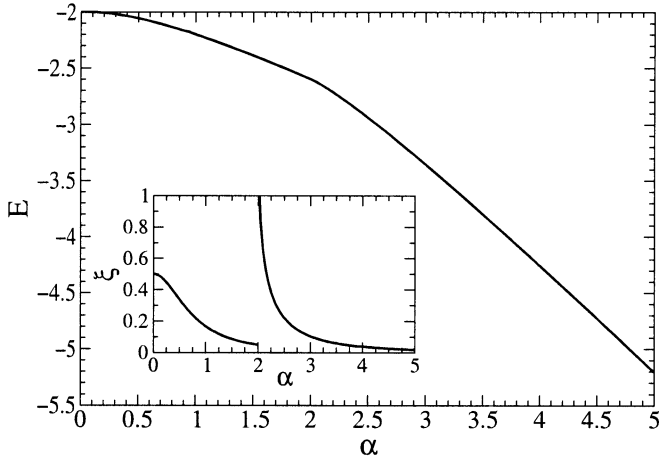
**Fig. 3.** The ground state energy as a function of the parameter $\alpha$. The inset shows the generalized stiffness $\xi$ as a function of the parameter $\alpha$



**Fig. 4.** The ground state magnetization as a function of the parameter $\alpha$. The inset shows the derivative of magnetization with respect to the parameter $\alpha$.

$\alpha > \alpha_c = 2$ corresponds to the phase transition in the ground state of the spin system. This transition is the second order quantum phase transition, which at the transition point is characterized by

- non-monotonic behavior of the ground state energy $E_0(\alpha)$ as a function of the parameter $\alpha$. In particular, the first derivative of the ground state energy with respect to the parameter $\alpha$ shows a kink, while the second derivative is divergent at $\alpha = \alpha_c$;
- magnetization of the system as a function of the parameter $\alpha$ shows the non-monotonic and nonanalytical behavior at $\alpha = \alpha_c$;
- the critical index characterizing the power-law decay of the transverse spin-spin correlation function is changed at $\alpha = \alpha_c$;
- At low temperature ($T \ll J$) the heat capacity, magnetization and magnetic susceptibility of the system show a well pronounced anomalous behavior at $\alpha \simeq \alpha_c$.

This quantum phase transition, despite its obviously rich nature, can be studied using the exact solution of the model (2), given in terms of *Fermi gas of spinless particles* (5).
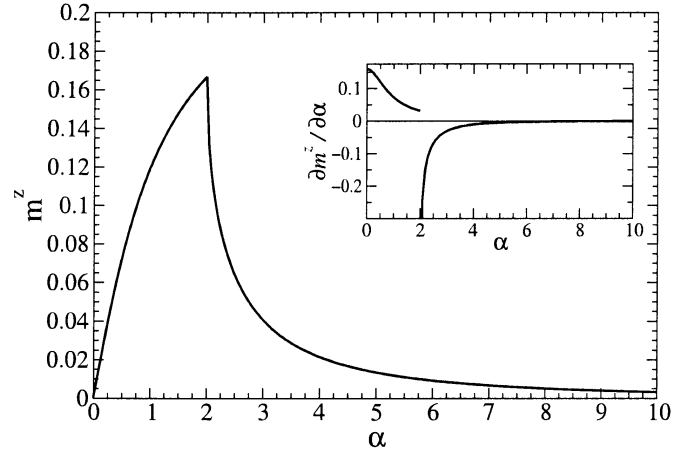
## 3 Phase transition in the ground state

The ground state energy of the system is given by

$$\mathcal{E}_0(\alpha) = \frac{L}{2\pi} \int_{\{\Lambda\}} \mathcal{E}(k) \mathrm{d}k \qquad (11)$$

where the integration region $\{\Lambda\} = [-k_F^-, k_F^-]$ for $\alpha < 2$ and $\{\Lambda\} = [-k_F^-, -k_F^+] \cup [k_F^+, k_F^-]$ for $\alpha > 2$.

In Figure 3 we plotted the ground-state energy of the system as a function of the parameter $\alpha$. At $\alpha = \alpha_c$ we observe (see inset in Fig. 3) the singularity in the behavior of the generalized stiffness

$$\xi(\alpha) = -\partial^2 \mathcal{E}_0(\alpha)/\partial^2 \alpha. \qquad$$

The singularity in $\xi(\alpha)$ we attribute to the second-order phase transition in the ground-state of the system with the increase of the three-spin coupling constant $J^* = \alpha J$.

### 3.1 Magnetization

Most clearly, the change of the properties of the system at the transition point is seen in the non-monotonic behavior of magnetization. At $T = 0$ the magnetization (per site) of the system is given by the number of SF in the ground state

$$m^z(\alpha) = \frac{1}{L} \sum_n \langle S_n^z \rangle = \begin{cases} k_F^-/\pi - 1/2 & \text{at } (\alpha < 2) \\ \left(k_F^- - k_F^+\right)/\pi - 1/2 & \text{at } (\alpha > 2). \end{cases} \qquad (12)$$

Using equations (9–10) we found that the ground-state of the system is singlet with $m^z = 0$ only at $\alpha = 0$ (the $XY$ model) and in the limiting case $\alpha = \infty$. For arbitrary nonzero $\alpha$, the magnetization of the system is finite. It is a monotonically increasing function of the parameter $\alpha$ in the range of $0 < \alpha < 2$ (see Fig. 4). It reaches its cusp-type maximum at $\alpha = 2$ with $m^z = 1/6$ and then monotonically decreases to zero with $\alpha \to \infty$.

The derivative of magnetization with respect to the parameter $\alpha$ (see Inset in the Fig. 4) is

$$\partial m^z(\alpha)/\partial \alpha \simeq \begin{cases} \text{const.} & \text{at } (\alpha - \alpha_c \to 0_-) \\ -\dfrac{1}{\sqrt{\alpha - \alpha_c}} & \text{at } (\alpha - \alpha_c \to 0_+). \end{cases} \qquad (13)$$

### 3.2 Correlation functions

To clarify the symmetry properties of various phases realized in the ground state of the system, we calculate the

longitudinal and transverse spin-spin correlation functions

$$\mathcal{K}^z(r) = \langle S_n^z S_{n+r}^z \rangle, \tag{14}$$

$$\mathcal{K}^{tr}(r) = \langle S_n^x S_{n+r}^x \rangle = \langle S_n^y S_{n+r}^y \rangle. \tag{15}$$

The spin-spin correlations in the case of ordinary $XY$ chain $(\alpha = 0)$ were studied in the classical paper by Lieb, Schulz and Mattice [6]. The longitudinal spin-spin correlation function is

$$\mathcal{K}^z(r) - m_z^2 \sim r^{-2}$$

and the transverse correlation function decays more slowly

$$\mathcal{K}^{tr}(r) \sim r^{-1/2}.$$

For further results on these correlation functions, see reference [11].

In our calculations of correlation functions we follow the route used in reference [6]. In this approach the correlation functions are given in terms of Toeplitz determinants. Using the Jordan-Wigner transformation (3) one can easily found that

$$\mathcal{K}^z(r) = \det \hat{\mathbf{g}} = \frac{1}{4} \begin{vmatrix} g(0) & g(r) \\ g(r) & g(0) \end{vmatrix} = \frac{1}{4} \left( g^2(0) - g^2(r) \right) \tag{16}$$

and

$$\mathcal{K}^{tr}(r) = \det \hat{\mathbf{G}} = \frac{1}{4} \begin{vmatrix} g(1) & g(2) & \dots & g(r) \\ g(0) & g(1) & \dots & g(r-1) \\ \dots & \dots & \dots & \dots \\ \dots & \dots & \dots & \dots \\ g(2-r) & g(3-r) & \dots & g(1) \end{vmatrix}. \tag{17}$$

Here

$$g(r) = \frac{2}{\pi r} \sin(k_F^- r) - \delta_{0r} \tag{18}$$

at $\alpha < \alpha_c$, and

$$g(r) = \frac{2}{\pi r} \left[ \sin(k_F^- r) - \sin(k_F^+ r) \right] - \delta_{0r} \tag{19}$$

at $\alpha > \alpha_c$.

After straightforward calculations we obtain that for $\alpha < \alpha_c$

$$\mathcal{K}^z(r) = m_z^2 - \frac{1}{\pi^2} \frac{\sin^2(k_F^- r)}{r^2} \tag{20}$$

and for $\alpha > \alpha_c$

$$\mathcal{K}^z(r) = m_z^2 - \frac{1}{\pi^2} \frac{\left( \sin(k_F^- r) - \sin(k_F^+ r) \right)^2}{r^2}. \tag{21}$$

As we observe, the quadratic decay of the longitudinal correlations remains unchanged at the transition point. However, the additional oscillations in the longitudinal correlation function $\sim\cos(2k_F^+ r)$ and $\sim\cos\left((k_F^- \pm k_F^+)r\right)$

associated with the presence of two Fermi points are clearly seen.

The transverse correlation undergoes more dramatic change. We obtain that, for $\alpha < \alpha_c$

$$\mathcal{K}^{tr}(r) = \frac{A}{r^{1/2}} + \frac{B \cos(2k_F^- r)}{r^{5/2}} \tag{22}$$

and for $\alpha > \alpha_c$.

$$\mathcal{K}^{tr}(r) = \frac{B_1 \cos(k_F^- r + \varphi_-))}{r} + \frac{C_1 \cos\left(k_F^+ r + \varphi_+\right)}{r}$$

$$+ \frac{D_1 \cos\left((2k_F^- - k_F^+)r + \varphi_1\right)}{r^3}$$

$$+ \frac{E_1 \cos\left((2k_F^+ - k_F^-)r + \varphi_2\right)}{r^3}. \tag{23}$$

Here $A = A(\alpha), ...E_1(\alpha)$ are the smooth functions of the parameter $\alpha$.

Below the gapless phase with the power-law decay of spin-spin correlations given by equations (20, 22) is called the *Spin Liquid I* (SL-I) phase, while the gapless phase with the power-law decay of spin-spin correlations given by equations (21, 23) – the *Spin Liquid II* (SL-II) phase.

The behavior of the correlation functions given by equations (20–23) perfectly fits into the usual conformal theory results for the systems with several gapless excitations [12,13].

## 3.3 Emptiness formation probability

The very important quantity which characterizes a quantum spin system in the spin-liquid phase is the so called emptiness formation probability (EFP) [14], *i.e.* the probability to find a ferromagnetic string of the length "$n$" in the spin liquid ground state

$$P(n) = \left\langle GS| \prod_{j=1}^n \left( S_j^z + \frac{1}{2} \right) |GS \right\rangle. \tag{24}$$

To calculate the EFP we follow the route developed in the recent paper by Siroishi *et al.* [15]. In the SF representation the EFP is described in terms of the following determinant
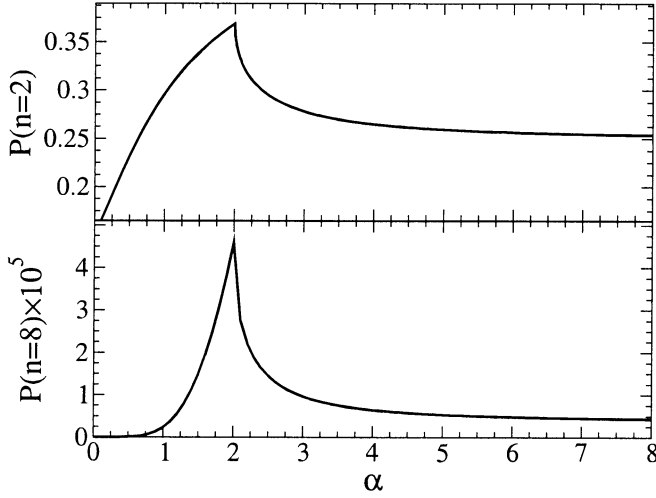
$$P(n) = \begin{vmatrix} f_{11} & f_{12} & \dots & f_{1n} \\ f_{21} & f_{22} & \dots & f_{2n} \\ \dots & \dots & \dots & \dots \\ \dots & \dots & \dots & \dots \\ f_{n1} & f_{n2} & \dots & f_{nn} \end{vmatrix}, \tag{25}$$

where

$$f_{nm} = \langle GS|c_n^\dagger c_m|GS \rangle = 1/(2\pi) \int_\Lambda \mathrm{d}q \exp(-iq(n-m)). \tag{26}$$

For $\alpha < \alpha_c$

$$f_{nm} = \frac{2}{\pi(n-m)} \sin(k_F^-(n-m)/2) \cos(k_F^-(n-m)/2) \tag{27}$$

**Fig. 5.** The emptiness formation probability $P(n)$ at $n = 2$ and $n = 8$ as a function of the parameter $\alpha$.

and for $\alpha > \alpha_c$

$$f_{nm} = \frac{1}{\pi(n-m)}[\sin(k_F^-(n-m)) - \sin(k_F^+(n-m))]$$

$$= \frac{2}{\pi(n-m)}\sin([k_F^- - k_F^+](n-m)/2)$$

$$\times \cos([k_F^- + k_F^+](n-m)/2). \qquad (28)$$

Using equations (25–28) we calculated the exact values of EFP $P(n)$ for $n = 1, ..., 20$. The results of these calculations are presented in the Table 1 (see Appendix A). In Figure 5 we plotted the EFP $P(n)$ as a function of the parameter $\alpha$ for $n = 2$ and $n = 8$. As it is clearly seen from this figure the EFP shows the nonmonotonic behavior at $\alpha = \alpha_c$.

To consider whether QPT leads to the change in the asymptotic $(n \to \infty)$ behavior of EFP we derived the analytical expressions for EFP at $\alpha < \alpha_c$ and $\alpha > \alpha_c$ which fit the numerical data.

At $\alpha < \alpha_c$, (in full agreement with the results obtained in the Ref. [15]) we obtain the following expression for EFP
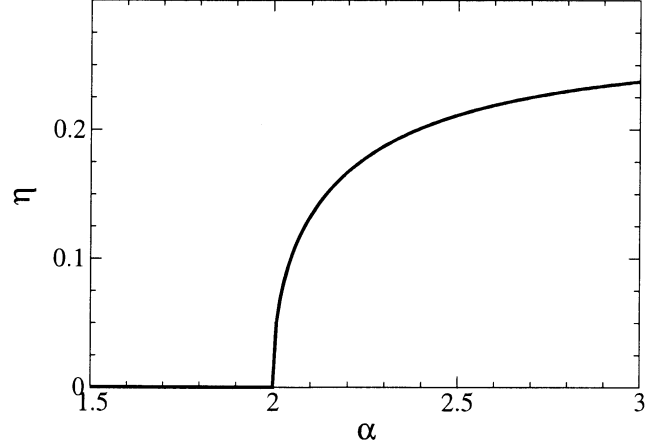
$$P_<(n) = C \left(\cos\frac{k_F^-}{2}\right)^{-1/4} n^{-1/4} \left(\sin\frac{k_F^-}{2}\right)^{n^2}, \qquad (29)$$

where $C = 0.6450$.

At $\alpha \gg \alpha_c$ we obtain the following expression for EFP, which fits our exact data

$$P_{>>}(n) = \left[\sin\left(\frac{k_F^- - k_F^+}{2}\right)\sin\left(\frac{k_F^- + k_F^+}{2}\right)\right]^{\frac{n^2}{2}}$$

$$\times \left(\frac{A_1 + (-1)^n B_1}{n^{1/2}}\right), \qquad (30)$$

where $A_1 = 0.659$ and $B_1 = 0.054$. In the intermediate regime, for $\alpha \geq \alpha_c$ the fitting formula is more complicated



**Fig. 6.** Order Parameter as a function of the parameter $\alpha$.

and is presented in Appendix B. As we see, the QPT in the system manifestly changes the EFP.

### 3.4 Order parameter

The QPT at $\alpha = \alpha_c$ from the SL-I to the SL-II phase requires an Order Parameter for complete description. As the order parameter we introduce the following quantity

$$\eta(\alpha) = \bar{\mathcal{L}}_{ExtXY} - \bar{\mathcal{L}}_{SL-I} \qquad (31)$$

where

$$\bar{\mathcal{L}}_{ExtXY} = \frac{\sum nP(n)}{\sum P(n)} \qquad (32)$$

is the average length of the ferromagnetic string in the ground state of the extended $XY$ chain with coupling $\alpha$ and, respectively, the magnetization $m^z(\alpha)$, while $\bar{\mathcal{L}}_{SL-I}$ is the same quantity calculated in the SL-I phases with the same value of the magnetization.

Straightforward calculations give (see Fig. 6)

$$\eta(\alpha) = \begin{cases} 0 & \text{at} \quad (\alpha - \alpha_c \to 0_-) \\ \sqrt{\alpha - \alpha_c} & \text{at} \ (\alpha - \alpha_c) \to 0_+). \end{cases} \qquad (33)$$

Thus, the order parameter exhibits the standard mean-field type behavior.

## 4 Thermodynamics

The QPT with respect to the parameter $\alpha$ in the ground-state of the system (2) is smeared out by thermal fluctuations at finite temperatures. Thus, the thermodynamic quantities have no singularities but, in the low-temperature region $T \ll J$ they show a well pronounced anomalous behavior at $|\alpha - \alpha_c| \ll T/J$.

To investigate the thermodynamics of the system let us first calculate the free energy. In the thermodynamic limit the free energy of the system is given by

$$F = -T \int d\omega \rho(\omega) \ln[2\cosh(\omega/2T)]. \qquad (34)$$

The SF density of states $\rho(\omega)$ is nonzero and equal to

$$\rho(\omega) = \rho^-(\omega) \tag{35}$$

for $\alpha < 2$ and for $\alpha > 2$ and $E(0) < \omega < W_{max}$. For $\alpha > 2$ and $W_{min} < \omega < E(0)$

$$\rho(\omega) = \rho^-(\omega) + \rho^+(\omega). \tag{36}$$

Here $W_{min} = \min\{-J(2 - \alpha)/2, -J(2\alpha^2 + 1)/4\alpha\}$, $W_{max} = J(\alpha + 2)/2$, and

$$\rho^{\pm}(\omega) = \frac{1}{\pi J} \frac{2\alpha}{\mathcal{G}_\alpha(\omega/J)} \frac{1}{\sqrt{4\alpha^2 - [1 \pm \mathcal{G}_\alpha(\omega/J)]^2}}, \tag{37}$$

where

$$\mathcal{G}_\alpha(\omega/J) = \sqrt{1 + 2\alpha^2 + 4\alpha(\omega/J)}. \tag{38}$$

Knowing the free energy it is easy to obtain the expression for the entropy

$$S = \int_{-\infty}^{\infty} d\omega \rho(\omega) \Big[ \ln\Big(2\cosh\Big(\frac{\omega}{2T}\Big)\Big) - \Big(\frac{\omega}{2T}\Big)\tanh\Big(\frac{\omega}{2T}\Big)\Big]. \tag{39}$$

Below in this section we study the anomalies in the low-temperature behavior of different thermodynamic quantities, caused by the presence of the QPT in the ground state at $\alpha \simeq \alpha_c$.

## 4.1 Specific heat

The anomalous temperature dependence in the vicinity of the QPT is seen most clearly in the low-temperature behavior of the specific heat. The heat capacity of the system is given by

$$C = \int_{-\infty}^{\infty} d\omega \rho(\omega) \frac{(\omega/2T)^2}{\cosh^2(\omega/2T)}. \tag{40}$$

Away from the critical point, the density of states in the vicinity of the Fermi level $\rho^-(0)$ at $\alpha \ll \alpha_c$ and $\rho^-(0) + \rho^+(0)$ at $\alpha \gg \alpha_c$, respectively, is the constant of the order of $\sim 1/J$. Therefore, in these cases the specific heat of the system
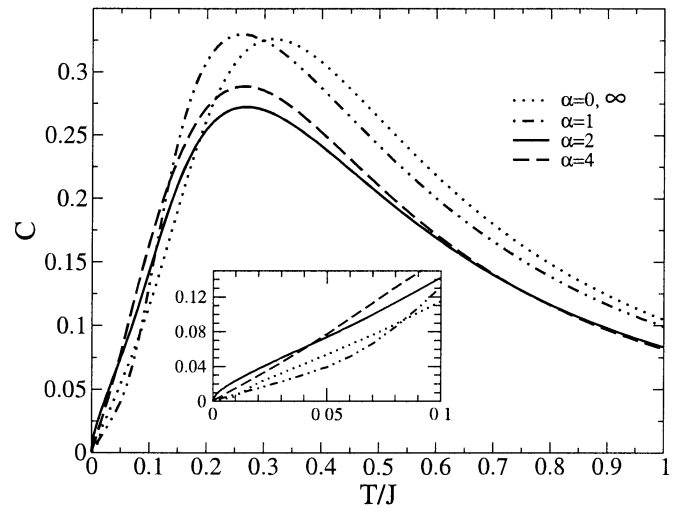
$$C(T) \simeq \gamma(T/J)$$

with $\gamma \sim 1$.

However, in the vicinity of the critical point, at $|\alpha - \alpha_c| \le |\omega/J|$,

$$\rho^+(\omega) \simeq \frac{1}{\pi\sqrt{6J|\omega|}} \tag{41}$$

and therefore, in this case the heat capacity of the system exhibits the anomalous square root dependence on the temperature

$$C = \gamma_1\sqrt{T/J} + \gamma(T/J). \tag{42}$$

In Figure 7 we plotted the heat capacity of the extended $XY$ model for different values of the parameter $\alpha$.



**Fig. 7.** The specific heat of the system as a function of the parameter $T/J$ for different values of the parameter $\alpha$. The inset shows the specific heat of the system at $T/J \ll 1$.

Since the bandwidth of the system depends on the parameter $\alpha$, in Figure 7 we plotted the results for the models with normalized bandwidth $W_R = 2J$. In the inset we present the low-temperature ($T \ll J$) heat capacity. The anomaly in the behavior of heat capacity at $\alpha = \alpha_c = 2$ is clearly seen.

## 4.2 Magnetization and magnetic susceptibility at T ≠ 0

At finite temperature the magnetization of the system is proportional to the average number of spinless fermions

$$m_\alpha^z(T) = -\frac{1}{2} \int_{-\infty}^{\infty} d\omega \rho(\omega) \tanh(\omega/2T), \tag{43}$$

while the magnetic susceptibility is given by

$$\chi(T) = \frac{1}{4T} \int_{-\infty}^{\infty} d\omega \rho(\omega) \frac{1}{\cosh^2(\omega/2T)}. \tag{44}$$

Let us first consider the limiting case of small temperatures $T/J \ll 1$. In this case it can be easily obtained, that for $\alpha \ll \alpha_c$
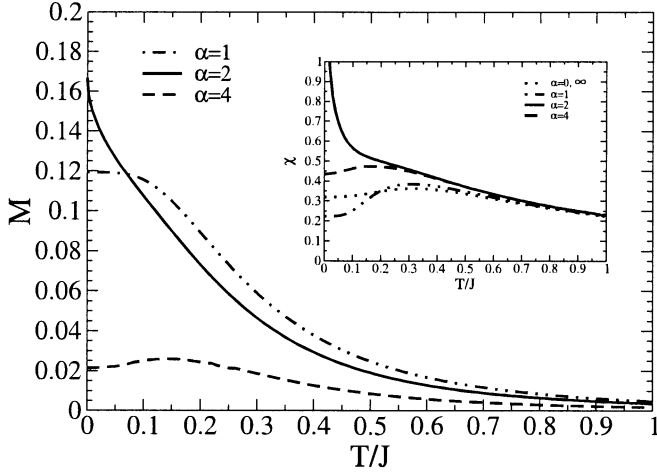
$$m_\alpha^z(T) = m_\alpha^z(0)\Big(1 - \frac{\pi^2}{2}(T/J)^2 + \mathcal{O}((T/J)^4)\Big), \tag{45}$$

$$\chi_\alpha(T) = \chi_\alpha(0)\Big(1 + \frac{\pi^2}{12}(T/J)^2 + \mathcal{O}((T/J)^4)\Big), \tag{46}$$

and for $\alpha \gg \alpha_c$

$$m_\alpha^z(T) = m_\alpha^z(0)\big(1 + 2\pi^2(T/J)^2 + \mathcal{O}((T/J)^4)\big), \tag{47}$$

$$\chi_\alpha(T) = \chi_\alpha(0)\Big(1 + \frac{2\pi^2}{3}(T/J)^2 + \mathcal{O}((T/J)^4)\Big). \tag{48}$$

**Fig. 8.** Magnetization of the system as a function of temperature for different values of the parameter $\alpha$. The inset shows the magnetic susceptibility of the system as a function of temperature for different values of the parameter $\alpha$.

- The low temperature ($T/J \ll 1$) expansion shows that magnetization of the system decays with temperature at $\alpha < \alpha_c$, and *magnetization of the system increase with the increase of the temperature* at $\alpha > \alpha_c$.
- The magnetic susceptibility of the system is finite both for $\alpha \ll \alpha_c$ and $\alpha \gg \alpha_c$ and shows the inverse square root dependence on temperature for $|\alpha - \alpha_c| \ll T/J$.

In the case of coupling close to the critical value, at $|\alpha - \alpha_c| \ll T/J$

$$m_\alpha^z(T) = m_\alpha^z(0)\Big[1 - \beta_{1/2}(T/J)^{1/2} - \beta_{3/2}(T/J)^{3/2}$$

$$- \beta_2(T/J)^2 + \mathcal{O}((T/J)^{5/2})\Big] , \qquad (49)$$

$$\chi(T) = \beta_{-1/2}(TJ)^{-1/2} + \rho_\alpha^-(\omega = 0) + \mathcal{O}(T/J)^2 . \quad (50)$$

Here

$$\beta_{1/2} = -\frac{\sqrt{2}-1}{\sqrt{12\pi}}\zeta(1/2) > 0 , \qquad (51)$$

$$\beta_{3/2} = \frac{\sqrt{2}-1}{96\sqrt{6\pi}}\zeta(3/2) > 0 , \qquad (52)$$

$$\beta_2 = \frac{\pi}{81\sqrt{3}} , \qquad (53)$$

$$\beta_{-1/2} = \frac{1}{\sqrt{6\pi}}(2\sqrt{2}-1)\zeta(-1/2) > 0 , \qquad (54)$$

and $\zeta(z)$ is the Riemann's zeta function.

Let us now consider in detail the problem of *anomalous temperature dependence* of magnetization for $\alpha > \alpha_c$. In Figure 8 we plotted the magnetization of the system as a function of temperature for three different values of the parameter $\alpha = 1, 2$ and $4$. From Figure 8 it is clearly seen that at $\alpha = 4$ the magnetization reaches its maximum at
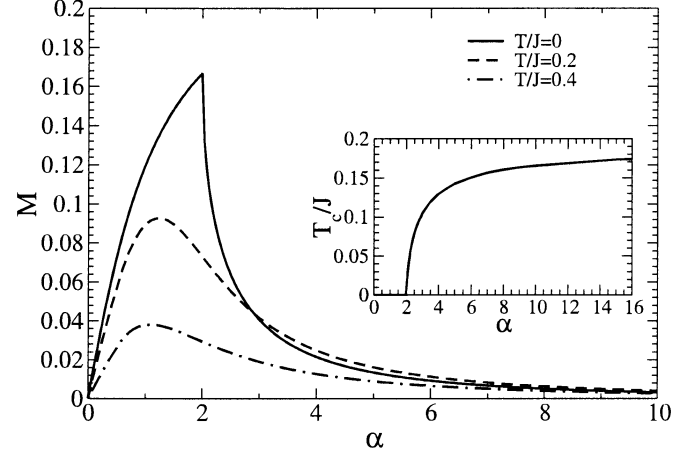


**Fig. 9.** Magnetization of the system as a function of the parameter $\alpha$ at different values of temperature.

$T = 0.15J$ and then smoothly decays with the increase of temperature.

To gain more insight into the behavior of magnetization in Figure 9 we plotted the magnetization as a function of the parameter $\alpha$ for different values of the temperature. As it is clearly seen from Figure 9, $M(T) < M_0 \equiv M(T = 0)$ at arbitrary $T$ when $\alpha < \alpha_c$. But at $\alpha > \alpha_c$ there does exist the *crossover temperature* $T_c$, and so $M(T) > M_0$ for $0 < T < T_c$ and $M(T) < M_0$ for $T > T_c$. We calculated $T_c$ as a function of the parameter $\alpha$ (see inset in Fig. 9) and found that $T_c$ monotonically increases with the increase of $\alpha$ from its minimum value $T_c = 0$ at $\alpha = \alpha_c = 2$ up to $T_c = 0.186J$ at $\alpha \to \infty$ .

The source of such unusual behavior is the structure of the excitation spectrum: at $\alpha \neq 0$ the ground state of the system is characterized by the magnetization $M_0^\alpha$. At $\alpha < \alpha_c$, the excited states with magnetization $M = M_0^\alpha \pm m$ have equal energy for arbitrary $m = 1, 2, ...$ Therefore, for $\alpha < \alpha_c$ at arbitrary finite temperature $M^\alpha(T) < M_0^\alpha$. On the other hand, for $\alpha > \alpha_c$ the excitation spectrum of the system exhibits a clear anisotropy: at least some lowest excited states with magnetization $M = M_0^\alpha + m$ (with $m = 1, 2..., m_0$) are far below their counterparts with magnetization $M = M_0^\alpha - m$. Therefore, at sufficiently low temperatures, where the states with magnetization $M > M_\alpha^0$ are occupied mainly, the total magnetization of the system increases. However, with further increase of the temperature, the difference in occupation of states with $M = M_\alpha^0 \pm m$ reduces, and finally, at $T > T_c$, the magnetization of the system drops below its ground state value.

# 5 Properties of the system in the presence of external magnetic field

In this section we consider the properties of the extended $XY$ spin chain (2) in the presence of an external magnetic field. We consider the general case, where the

field dependent part of the Hamiltonian is given by

$$\mathcal{H} = -\sum_n \left( H_0 + (-1)^n H_\delta \right) S_n^z. \tag{55}$$

In terms of spinless Fermions the Hamiltonian of the extended $XY$ model in the presence of an external magnetic field reads

$$\mathcal{H} = -\frac{J}{2} \sum_n \left( c_n^\dagger c_{n+1} + c_{n+1}^\dagger c_n \right)$$

$$+ \frac{J^*}{4} \sum_n \left( c_n^\dagger c_{n+2} + c_{n+2}^\dagger c_n \right)$$

$$- \sum_n \left( H_0 + (-1)^n H_\delta \right) \left( c_n^\dagger c_n - \frac{1}{2} \right). \tag{56}$$

Below in this section we consider separately the ground state phase diagram of the extended $XY$ spin chain in the case of:

- applied uniform magnetic field $H_\delta = 0$;
- applied staggered magnetic field $H_0 = 0$;
- applied magnetic field acting only on the spins on the even sites $H_0 = H_\delta = H$.

## 5.1 Uniform magnetic field

In the case of applied uniform magnetic field ($H_\delta = 0$, $H_0 = hJ$) the diagonalization of the Hamiltonian is straightforward and gives

$$\mathcal{H} = \sum_k E_1(k) c^\dagger(k) c(k) \tag{57}$$

where

$$E_1(k) = -J \left( h + \cos(k) - \frac{\alpha}{2} \cos 2k \right). \tag{58}$$
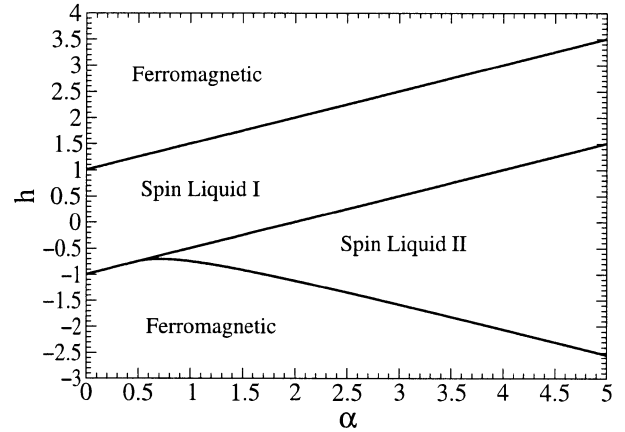
The phase diagram of the model in the case of applied uniform magnetic field is presented in Figure 10:

- For $hJ < W_{min}$ and $hJ > W_{max}$ the system is in the *ferromagnetic phase.*
- For $-\left(1 - \frac{1}{2}\alpha\right) < h < \left(1 + \frac{1}{2}\alpha\right)$ the system is in the *SL-I* phase.
- For $\alpha > 0.5$ and $-\left(2\alpha^2 + 1\right)/4\alpha < h < -\left(1 - \frac{1}{2}\alpha\right)$ the system is in the *SL-II* phase.

## 5.2 Staggered magnetic field

In the case of applied staggered magnetic field ($H_0 = Jh$, $H_\delta = Jh_\delta$) it is useful to introduce two types of spinless fermions determined on the odd and even sub-lattices, respectively

$$c_{2n-1} \equiv a_{n-1/2} \quad \text{and} \quad c_{2n} \equiv b_n. \tag{59}$$

**Fig. 10.** The ground state phase diagram of the model in the case of applied uniform magnetic field.

In terms of these new particles, the Hamiltonian in the momentum space reads

$$\mathcal{H} = \sum_k \left[ \left( \varepsilon_a(k) a_k^\dagger a_k + \varepsilon_b(k) b_k^\dagger b_k + \varepsilon_{ab}(k) \left( a_k^\dagger b_k + b_k^\dagger a_k \right) \right) \right] \tag{60}$$

where

$$\varepsilon_a(k) = \frac{J^*}{2} \cos(2k) - h_0 + h_\delta,$$

$$\varepsilon_b(k) = \frac{J^*}{2} \cos(2k) - h_0 - h_\delta,$$

$$\varepsilon_{ab}(k) = -J \cos k. \tag{61}$$

Using the standard Bogoliubov rotation

$$a_k = \cos\left(\frac{1}{2}\theta_k\right) \alpha_k + \sin\left(\frac{1}{2}\theta_k\right) \beta_k$$

$$b_k = -\sin\left(\frac{1}{2}\theta_k\right) \alpha_k + \cos\left(\frac{1}{2}\theta_k\right) \beta_k \tag{62}$$

where

$$\tan(\theta_k) = \frac{2\varepsilon_{ab}(k)}{\varepsilon_a(k) - \varepsilon_b(k)} \tag{63}$$

we finally obtain

$$\mathcal{H} = \sum_k \left( E_-(k) \alpha_k^\dagger \alpha_k + E_+(k) \beta_k^\dagger \beta_k \right), \tag{64}$$

where

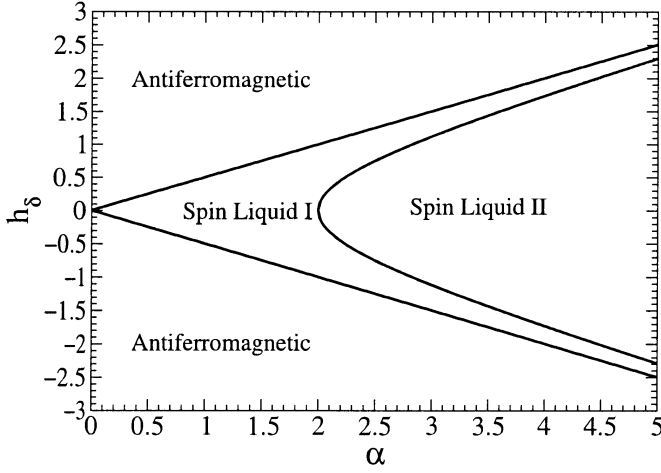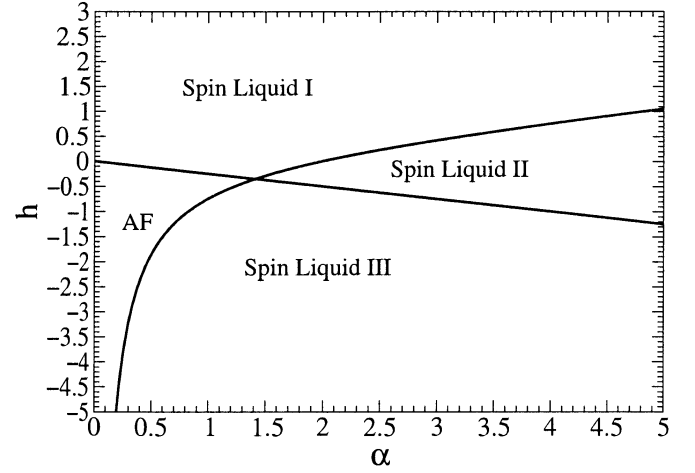$$E_\pm(k) = J \left( \frac{\alpha}{2} \cos 2k - h \pm \sqrt{h_\delta^2 + \cos^2 k} \right). \tag{65}$$

Let us first consider the case of the staggered magnetic field ($H_0 = 0$). The ground state phase diagram of the model in this case consists of the following four sectors (see Fig. 11):

- At $|h_\delta| > \frac{1}{2}\alpha$ the system is in the long-range ordered Neél *anti-ferromagnetic phase.*

**Fig. 11.** The ground state phase diagram of the model in the case of applied staggered magnetic field.



**Fig. 12.** Phase diagram for Uniform Magnetic field + alternating Magnetic field

There is a gap in the spin excitation spectrum. The longitudinal spin-spin correlation function is

$$\mathcal{K}_z(r) = \langle S_n^z S_{n+r}^z \rangle \simeq (-1)^r f(\alpha)$$

where $f(\alpha)$ is the constant of the order of unity for given $\alpha$.

- At $\alpha < 2$ and $|h_\delta| < \frac{1}{2}\alpha$ as well as for $\alpha > 2$ and $\sqrt{\frac{\alpha^2-4}{4}} < |h_\delta| < \frac{1}{2}\alpha$ the system is in the *SL-I* phase;

- At $\alpha > 2$ and $|h_\delta| < \sqrt{\frac{\alpha^2-4}{4}}$ the system is in the *SL-II* phase.

## 5.3 Mixed magnetic field

In this subsection we consider a rather special case, where the mixed magnetic field with equal strength of the uniform and staggered components $H_0 = H_\delta = hJ$. This corresponds to the case, where the magnetic field of the $2hJ$ strength is applied to the spins on the even sites, while the spins on the odd sites experience no magnetic field.

The spectrum of the system in this case is given by

$$\tilde{E}_2^\pm(k) = J\left(\frac{\alpha}{2}\cos 2k - h \pm \sqrt{h^2 + \cos^2 k}\right). \qquad (66)$$

The ground state phase diagram of the model (60) in the case of applied mixed magnetic field consists of the following four sectors (see Fig. 12)

- At $\alpha < \sqrt{2}$ and $-\frac{4-\alpha^2}{4\alpha} < h < -\frac{1}{4}\alpha$ the system is in the long-range ordered Neél *antiferromagnetic phase*;
- At $\alpha > \sqrt{2}$ and $-\frac{1}{4}\alpha < h < -\frac{4-\alpha^2}{4\alpha}$ the system is in the *SL-II* phase;
- At $h > \max\{-\frac{1}{4}\alpha; -\frac{4-\alpha^2}{4\alpha}\}$ the system is in the *SL-I* phase;
- At $h < \min\{-\frac{1}{4}\alpha; -\frac{4-\alpha^2}{4\alpha}\}$ the system is in the *SL-III* phase.

The new *SL-III* phase corresponds to the gapless phase characterized by qualitatively different behavior of the long-range spin-spin correlations for the spins located on the even and odd sites. The calculation of the longitudinal spin-spin correlations between the spins on the even sites gives

$$\mathcal{K}_{0,2m}^z(r = 2m) = (m_z^{even})^2, \qquad (67)$$

between the spins on the odd sites

$$\mathcal{K}_{1,2m+1}^z(r = 2m) = (m_z^{odd})^2 - \frac{B}{r^2}, \qquad (68)$$

and between the spins on even and odd sites

$$\mathcal{K}_{1,2m}^z(r = 2m - 1) = m_z^{even} m_z^{odd} \qquad (69)$$

respectively. Here $m_z^{even} < 0$ and $m_z^{odd} > 0$ is the magnetization per site of the even and odd sub-lattices, respectively, which is calculated at the given value of the coupling $\alpha$. The parameter $B$ is a smooth function of the coupling constant $\alpha$ and at the given $\alpha$ it is the constant of the order of unity. For example, at $h = -0.4$ and $\alpha = 1.5$ $m_z^{even} = -0.3406$ and $m_z^{odd} = 0.1690$. Therefore, in the SL-III phase, we have antiferromagnetically coupled two ferromagnetically ordered sub-lattices.

In the SL-III phase the transverse correlations also show the unusual behavior. In particular, the transverse spin correlation between the spins on the even sites is

$$\mathcal{K}_{0,2m}^{tr}(r = 2m) = 0, \qquad (70)$$

between the spin on the odd sites

$$\mathcal{K}_{1,2m+1}^{tr}(r = 2m) \simeq \frac{(-1)^m}{r^{1/2}}, \qquad (71)$$

and between the spins on the even and odd sites

$$\mathcal{K}_{1,2m}^{tr}(r = 2m - 1) \simeq \frac{(-1)^m}{r^{3/2}}. \qquad (72)$$

**Table 1.** The emptiness formation probability $P(n)$.

| | $\alpha = 0$ | $\alpha = 1$ | $\alpha = 2$ | $\alpha = 4$ | $\alpha = \infty$ |
|---|---|---|---|---|---|
| | $\langle m^z \rangle = 0$ | $\langle m^z \rangle = 0.1193$ | $\langle m^z \rangle = 1/6$ | $\langle m^z \rangle = 0.0213387$ | $\langle m^z \rangle = 0$ |
| $n = 1$ | 0.5 | $6.1928 \times 10^{-1}$ | $6.6667 \times 10^{-1}$ | $5.2134 \times 10^{-1}$ | 0.5 |
| $n = 2$ | $1.4868 \times 10^{-1}$ | $2.9576 \times 10^{-1}$ | $3.6845 \times 10^{-1}$ | $2.6455 \times 10^{-1}$ | 0.25 |
| $n = 3$ | $2.3679 \times 10^{-2}$ | $1.0251 \times 10^{-1}$ | $1.6136 \times 10^{-1}$ | $8.4078 \times 10^{-2}$ | $7.4339 \times 10^{-2}$ |
| $n = 4$ | $1.9453 \times 10^{-3}$ | $2.5041 \times 10^{-2}$ | $5.4640 \times 10^{-2}$ | $2.5783 \times 10^{-2}$ | $2.2105 \times 10^{-2}$ |
| $n = 5$ | $8.1263 \times 10^{-5}$ | $4.2525 \times 10^{-3}$ | $1.4127 \times 10^{-2}$ | $4.5135 \times 10^{-3}$ | $3.5205 \times 10^{-3}$ |
| $n = 6$ | $1.7152 \times 10^{-6}$ | $4.9869 \times 10^{-4}$ | $2.7702 \times 10^{-3}$ | $7.6228 \times 10^{-4}$ | $5.6069 \times 10^{-4}$ |
| $n = 7$ | $1.8232 \times 10^{-8}$ | $4.0241 \times 10^{-5}$ | $4.1052 \times 10^{-4}$ | $7.0945 \times 10^{-5}$ | $4.6062 \times 10^{-5}$ |
| $n = 8$ | $9.7402 \times 10^{-11}$ | $2.2298 \times 10^{-6}$ | $4.5877 \times 10^{-5}$ | $6.3746 \times 10^{-6}$ | $3.7841 \times 10^{-6}$ |
| $n = 9$ | $2.6122 \times 10^{-13}$ | $8.4729 \times 10^{-8}$ | $3.8609 \times 10^{-6}$ | $3.1110 \times 10^{-7}$ | $1.5808 \times 10^{-7}$ |
| $n = 10$ | $3.5137 \times 10^{-16}$ | $2.2060 \times 10^{-9}$ | $2.4448 \times 10^{-7}$ | $1.4664 \times 10^{-8}$ | $6.6036 \times 10^{-9}$ |
| $n = 11$ | $2.3691 \times 10^{-19}$ | $3.9329 \times 10^{-11}$ | $1.1641 \times 10^{-8}$ | $3.7291 \times 10^{-10}$ | $1.3938 \times 10^{-10}$ |
| $n = 12$ | $8.0036 \times 10^{-23}$ | $4.7992 \times 10^{-13}$ | $4.1656 \times 10^{-10}$ | $9.1615 \times 10^{-12}$ | $2.9420 \times 10^{-12}$ |
| $n = 13$ | $1.3543 \times 10^{-26}$ | $4.0070 \times 10^{-15}$ | $1.1200 \times 10^{-11}$ | $1.2099 \times 10^{-13}$ | $3.1272 \times 10^{-14}$ |
| $n = 14$ | $1.1475 \times 10^{-30}$ | $2.2884 \times 10^{-17}$ | $2.2619 \times 10^{-13}$ | $1.5439 \times 10^{-15}$ | $3.3240 \times 10^{-16}$ |
| $n = 15$ | $4.8677 \times 10^{-35}$ | $8.9382 \times 10^{-20}$ | $3.4304 \times 10^{-15}$ | $1.0568 \times 10^{-17}$ | $1.7758 \times 10^{-18}$ |
| $n = 16,$ | $1.0336 \times 10^{-39}$ | $2.3871 \times 10^{-22}$ | $3.9063 \times 10^{-17}$ | $6.9905 \times 10^{-20}$ | $9.4872 \times 10^{-21}$ |
| $n = 17$ | $1.0984 \times 10^{-44}$ | $4.3587 \times 10^{-25}$ | $3.3395 \times 10^{-19}$ | $2.4771 \times 10^{-22}$ | $2.5443 \times 10^{-23}$ |
| $n = 18$ | $5.8409 \times 10^{-50}$ | $5.4406 \times 10^{-28}$ | $2.1431 \times 10^{-21}$ | $8.4825 \times 10^{-25}$ | $6.8235 \times 10^{-26}$ |
| $n = 19$ | $1.5534 \times 10^{-55}$ | $4.6420 \times 10^{-31}$ | $1.0323 \times 10^{-23}$ | $1.5538 \times 10^{-27}$ | $9.1783 \times 10^{-29}$ |
| $n = 20$ | $2.0604 \times 10^{-61}$ | $2.7070 \times 10^{-34}$ | $3.7316 \times 10^{-26}$ | $2.7538 \times 10^{-30}$ | $1.2346 \times 10^{-31}$ |

# 6 Conclusion

In conclusion, we investigated the ground state phase diagram and the low-temperature thermodynamics of the extended $XY$ model with nearest-neighbor exchange ($J$) and three-spin interaction $J^* = \alpha J$. At $J^* \neq 0$ the spin system is characterized by the broken time reversal symmetry and for arbitrary $\alpha \neq 0, \infty$ shows a finite magnetization in the ground state $M^0(\alpha)$. We have shown that with the increase of the three-spin coupling the Quantum Phase Transition from the Spin-Liquid-I into the Spin-Liquid-II phase takes place. In the Spin-Liquid-I phase, at $\alpha < \alpha_c^* = 2$ the properties of the extended $XY$ chain are similar to those of the standard $XY$ model in the presence of such an "effective" magnetic field that ensures the same value of the GS magnetization $M^0$. However, in the Spin-Liquid-II phase, at $\alpha > \alpha_c$, the behavior of the magnetization, magnetic susceptibility, emptiness formation probability and different spin-spin correlation functions is qualitatively different and could not be considered by the simple effect of an "effective" magnetic field. The anomalous behavior of the heat capacity of the system, entropy, magnetization and magnetic susceptibility connected with the presence of QPT in the ground state has been shown. The ground state phase diagram of the model in the case of applied uniform and/or staggered magnetic field has been also obtained.

# Appendix A

In this appendix we present the exact values of the EFP $P(n)$ for different values of the parameter $\alpha$, obtained by evoluation of the Toeplitz determinant (25).

**Table 2.** The coefficients of the fitting formula (73) for the emptiness formation probability $P(n)$ for different values of the parameter $\alpha > \alpha_c$.

| $\alpha$ | $A_1$ | $B_1$ | $C_1$ | $D_1$ |
|---|---|---|---|---|
| 2.005 | 0.155 | 0.009 | 0.302 | 0.314 |
| 2.01 | 0.204 | 0.011 | 0.370 | 0.194 |
| 2.05 | 0.331 | 0.018 | 0.350 | 0.072 |
| 2.1 | 0.351 | 0.021 | 0.322 | 0.063 |
| 2.2 | 0.572 | 0.032 | 0.150 | 0.021 |
| 2.3 | 0.673 | 0.037 | 0.064 | $-0.003$ |
| 2.4 | 0.683 | 0.039 | 0.045 | $-0.006$ |
| 2.5 | 0.685 | 0.041 | 0.036 | $-0.006$ |
| 3 | 0.682 | 0.045 | 0.012 | $-0.005$ |
| 4 | 0.675 | 0.050 | $-0.0002$ | $-0.004$ |
| 10 | 0.662 | 0.053 | $-0.006$ | $-0.003$ |
| $\infty$ | 0.661 | 0.054 | 0 | 0 |

## Appendix B

In this appendix we present the expression for the EFP, which fits our exact data for $\alpha \geq \alpha_c$:

$$P_>(n) = \left[ \sin\left( \frac{k_F^- - k_F^+}{2} \right) \sin\left( \frac{k_F^- + k_F^+}{2} \right) \right]^{\frac{n^2}{2}}$$

$$\times \left( \frac{A_1 + (-1)^n B_1}{n^{1/2}} + \frac{C_1 + D_1 \cos(k_F^+ n)}{n^{1/4}} \right). \quad (73)$$

For different values of the parameters $\alpha$ the fitting values of the coefficients $A_1, ... D_1$ are given in Table 2.

## References

1. S. Sachdev, *Quantum Phase Transitions* (Cambridge University Press, Cambridge, 1999)
2. M. Fabrizio, Phys. Rev. B **54**, 10054 (1996)
3. R. Arita, K. Kuroki, H. Aoki, M. Fabrizio, Phys. Rev. B **57**, 10324 (1998)
4. S. Daul, R.M. Noack, Phys. Rev. B **61**, 1646 (2000)
5. C. Aebischer, D. Baeriswyl, R.M. Noack, Phys. Rev. Lett. **86**, 468 (2001)
6. E.H. Lieb, T. Schulz, D. Mattis, Ann. Phys. (N.Y.) **16**, 417 (1961)
7. S. Katsura, Phys. Rev. **127**, 1508 (1662)
8. M. Takahashi, *Thermodynamics of One Dimensional Solvable Models* (Cambridge University Press, Cambridge, 1999)
9. M. Suzuki, Phys. Lett. A **34**, 94 (1971); Prog. Theor. Phys. **46**, 1337 (1971)
10. P. Jordan, E. Wigner, Z. Phys. **47**, 631 (1928)
11. V.E. Korepin, A.G. Izergin, N.M. Bogoliubov, *Quantum Inverse Scattering Method and Correlation Functions* (Cambridge University Press, Cambridge, 1993)
12. H. Frahm, J. Phys. A **25**, 1417 (1992)
13. A.A. Zvyagin, A. Klümper, J. Zittartz, Eur. Phys. J. B **19**, 25 (2001)
14. V.E. Korepin, A.G. Izergin, F.H.L. Essler, D.B. Uglov, Phys. Lett. A **190**, 182 (1994)
15. M. Siroishi, M. Takahashi, I. Nishiyama, J. Phys. Soc. Jpn **70**, 3535 (2001)
16. M. Takahashi, Prog. Theor. Physics **51**, 1348 (1974)